SARS-CoV-2 receptor Angiotensin I-Converting Enzyme type 2 is expressed in human pancreatic islet β-cells and is upregulated by inflammatory stress

Daniela Fignani[1,2*], Giada Licata[1,2*], Noemi Brusco[1,2], Laura Nigi[1,2], Giuseppina E. Grieco[1,2], Lorella Marselli[4], Lut Overbergh[5], Conny Gysemans[5], Maikel L. Colli[6], Piero Marchetti[4], Chantal Mathieu[5], Decio L. Eizirik[6,7], Guido Sebastiani[1,2#] and Francesco Dotta[1,2,3#]

1. Diabetes Unit, Department of Medicine, Surgery and Neurosciences, University of Siena, Siena, Italy

2. Fondazione Umberto Di Mario, c/o Toscana Life Sciences, Siena, Italy.

3. Tuscany Centre for Precision Medicine (CReMeP), Siena, Italy.

4. Department of Clinical and Experimental Medicine, University of Pisa, Pisa, Italy.

5. Clinical and Experimental Endocrinology (CEE), Katholieke Universiteit Leuven (KULEUVEN), Leuven, Belgium.

6. ULB Center for Diabetes Research, Medical Faculty, Université Libre de Bruxelles, Brussels, Belgium.

7. Indiana Biosciences Research Institute, Indianapolis, Indiana, USA.

* Joint first co-authorship
# Share last co-authorship

Correspondence:

Prof. Francesco Dotta, MD

Department of Medicine, Surgery and Neurosciences

University of Siena

francesco.dotta@unisi.it

+39-0577-586269

Highlights

- **Human pancreatic islets express SARS-CoV-2 receptor Angiotensin I-Converting Enzyme type 2 (ACE2)**

- **In human pancreatic islets, ACE2 is preferentially expressed by β-cells**

- **In human β-cells, ACE2 expression is increased upon inflammatory stress**

Summary

Increasing evidence demonstrated that the expression of Angiotensin I-Converting Enzyme type 2 (ACE2), is a necessary step for SARS-CoV-2 infection permissiveness. In the light of the recent data highlighting an association between COVID-19 and diabetes, a detailed analysis aimed at evaluating ACE2 expression pattern distribution in human pancreas is still lacking. Here, we took advantage of INNODIA network EUnPOD biobank collection to thoroughly analyse ACE2, both at mRNA and protein level, in multiple human pancreatic tissues and using several methodologies. We showed that ACE2 is indeed present in human pancreatic islets, where is preferentially expressed by insulin producing β-cells. Of note, pro-inflammatory cytokines increased ACE2 expression in β-cells, thus putatively suggesting an enhancement of β-cells sensitivity to SARS-CoV-2 during inflammatory conditions. Taken together, our data indicate a potential link between SARS-CoV-2 infection and diabetes, through direct β-cell virus tropism.

Introduction

The host expression of molecules that act as receptors for viral attachment and/or entry are major determinants of viral tropism. SARS-coronavirus 2 (SARS-CoV-2), that leads to the respiratory illness coronavirus disease 2019 (COVID-19), uses its surface envelope Spike glycoprotein (S-protein) to interact and gain access to host cells through the Angiotensin-I converting enzyme-2 (ACE2) receptor. As such, S-protein-ACE2 binding is the key determinant for virus entry, propagation, and transmissibility of COVID-19-related disease (Lan et al., 2020; Shang et al., 2020).

Artificially induced ACE2 *de-novo* expression in ACE2-negative cell lines is a necessary step to SARS-CoV and SARS-CoV-2 infection and virus replication (Letko et al., 2020; Mossel et al., 2005). SARS-CoV-2 does not enter cells that do not express ACE2 and does not use other coronaviruses receptors, such as aminopeptidase N (APN) and dipeptidyl peptidase 4 (DPP4), thus being fully dependent on ACE2 presence in host cells (Zhou et al., 2020). Additional host co-factors, such as transmembrane protease TMPRSS2, cathepsin B/L and furin protease, have been shown to enhance replication efficiency of SARS-CoV-2 by processing the S-protein and eliciting membrane fusion and syncytia formation (Hou et al., 2020). The central role played by ACE2 in SARS-CoV-2 infection has been further supported by evidence that the SARS-CoV-2 infection titers are driven by ACE2 expression level (Hou et al., 2020). SARS-CoV-2 mainly targets cells of the lung epithelium, causing respiratory-related symptoms, but growing evidence show that other tissues can also be infected.

Several reports indicate a wide but variable distribution of ACE2 expression patterns among different tissues (Hamming et al., 2004; Hikmet et al., 2020; Li et al., 2020), thus underlining a potential different virus infection susceptibility among cell types. The fact that COVID-19 disease may lead to multiple organ failure (Cao et al., 2020; Guan et al., 2020) shows the crucial relevance for understanding the molecular mechanisms of host cell factors used by SARS-CoV-2 to infect their target tissues.

Recent studies showed that older adults and those with chronic medical conditions like heart and lung disease, and/or diabetes are at the highest risk for complications from SARS-CoV-2 infection. Of importance, a yet unresolved conundrum relies on the recently hypothesized bidirectional relationship between COVID-19 and diabetes mellitus (Gupta et al., 2020; Rubino et al., 2020). This concept is supported by reports in which impaired glycaemic control is associated with increased risk of severe COVID-19. Indeed, elevated blood glucose concentration and deterioration of glycaemic control may contribute to increased inflammatory response, abnormalities in the coagulation system and impairment of ventilatory function, thus leading to severe COVID-19 disease and to a worse prognosis (Zhu et al., 2020). Interestingly, acute hyperglycaemia has been observed at admission in a substantial percentage of SARS-CoV-2 infected subjects, regardless of the past medical history of diabetes (Chen et al., 2020; Iacobellis et al., 2020; Sardu et al., 2020; Wu et al., 2020). The same observations were previously made in SARS-CoV-1 pneumonia during 2003 SARS epidemic (Yang et al., 2010). This indicates the possibility of a link between SARS-CoV-2 infection and new onset diabetes through potential direct infection of pancreatic islets.

To address this question, we screened the ACE2 expression pattern in human pancreata obtained from non-diabetic multiorgan donors and in the insulin-producing human beta-cell line EndoC-βH1, using different methodologies and available datasets. Our data indicate that a subset of human β-cells preferentially express ACE2, thus being potentially prone to SARS-CoV-2 infection. More importantly, exposure of EndoC-βH1 human beta-cell line and human pancreatic islets to pro-inflammatory cytokines significantly increased ACE2 upregulation. Taken together, our data suggest that there may be a potential link between SARS-CoV-2 infection and new onset diabetes, which deserves further investigation based on long-term follow up of patients recovered from Covid-19 disease.

Results

ACE2 expression pattern in human pancreas

To determine the ACE2 protein expression pattern in human pancreatic tissue, we first performed a colorimetric immunohistochemistry analysis to detect ACE2 on formalin-fixed paraffin embedded (FFPE) pancreatic sections obtained from seven non-diabetic multiorgan donors (**Table S1**). To specifically detect ACE2 protein in such context, we used a previously validated monoclonal anti-human ACE2 antibody which is less likely to cross react with other proteins as compared to polyclonal ones (see Key Resources Table). For each pancreas, two sections derived from different FFPE tissue blocks were analyzed. Based on pancreas morphometry and histological composition, we identified three main cell types positive for ACE2 (**Fig. 1A, panel-a to -f**). In the exocrine pancreas there was a marked staining in a subset of vascular components (endothelial cells or pericytes) found in inter-acini septa (**Fig. 1A, panel-a and -b**). Such pattern clearly overlaps with CD31-positive endothelial cells specific staining in human pancreas (https://www.proteinatlas.org/ENSG00000261371-PECAM1/tissue/pancreas#img), suggesting association with vasculature and confirming the specificity of our immunohistochemistry results. Of note, a lobular staining pattern of ACE2 residing in endothelial cells/pericytes component was evident as demonstrated by the presence of positive cells in certain lobules and low or null expression in other lobules of the same pancreas section (**Fig. 1B**).

In line with previous studies, we also identified ACE2 positive cells in the pancreatic ducts, even though only some rare scattered cells with a marked ACE2 signal were detected (**Fig. 2A, panel-c and -d**).

Of interest, there was a clear ACE2 staining pattern in the endocrine pancreatic islets, showing a specific and pronounced ACE2 signal in a subset of cells within islet parenchyma (**Fig. 2A, panel -e**

and -f). In all cases analysed, including different blocks of the same case, a similar expression pattern of ACE2 was observed, with no clear marked differences based on age, gender or BMI (**Fig. S1 and Table S1**).

ACE2 is preferentially expressed in human β-cells

To determine which pancreatic islet cell subset contributes to ACE2 signal in the endocrine pancreas, we performed a triple immunofluorescence analysis on the same set of FFPE pancreatic sections of non-diabetic multiorgan donors, aimed at detecting glucagon-positive α-cells, insulin-positive β-cells and ACE2 signals (**Fig 2**). ACE2 preferentially overlapped with the insulin-positive β-cells (**Fig. 2A, panel-a to -m**), being mostly colocalized with insulin and low/not detectable in α-cells (**Fig 2A, panel-e, -f, -l , -m**). Such staining pattern was observed in all cases and was consistent between different blocks of the same case (**Table S2**). As expected, ACE2-only positive cells within or around the pancreatic islets were also observed (**Fig 2 A, panel g**), potentially indicating the presence of pericytes or endothelial cells interspersed in the islet parenchyma or surrounding it.

Intriguingly, a punctuate/granular signal residing in the β-cells, and partially overlapping with insulin positive granular one, was evident (**Fig. 2B, panel a-c and Fig. 2S**). On the contrary, ACE2-positive signal deriving from putative endothelial cells/pericytes, was mainly observed in plasma membrane (**Fig 2A, panel g)**, in line to what was previously observed in such and other cellular contexts (Wang et al., 2008).

Colocalization rate analysis between ACE2-insulin and ACE2-glucagon, performed on a total of 128 single pancreatic islets from seven different cases, confirmed the significant preferential expression of ACE2 in β-cells compared to α-cells (ACE2-INS 59.0 ± 20.2% vs. ACE2-GCG 7.7 ± 5.4%, $p<0.0001$) (**Fig. 2C and Fig S3**). There was however heterogeneity in terms of the ACE2-insulin colocalization

rate among different islets (ACE2-INS colocalization rate range: 10.7 – 91.3%). The comparison of co-localization rates between ACE2-insulin and ACE2-glucagon colocalization among all cases analysed, confirmed the consistent preferential expression of ACE2 in β-cells in comparison to α-cells (**Fig. 2C**). These results were confirmed when comparing different blocks of the same case (**Table S2**). Of note, some cases showed a lower ACE2-insulin mean colocalization rate compared to the other ones (**Fig. 2C**), thus suggesting heterogeneity also among cases in terms of ACE2 expression. Such heterogeneity was also highlighted by the presence of ACE2-negative pancreatic islets in the same pancreas section, even though they represented a minor fraction of the islets pool (data not shown). Collectively, these data indicate that ACE2 protein is expressed in different components of the pancreatic tissue, including a subset of pancreatic endocrine insulin-producing cells. This suggests a preferential tropism of SARS-CoV-2 to a subset of β-cells, but it remains to be determined what defines these susceptible cells.

ACE2 mRNA is expressed in human pancreatic islets and in the human beta-cell line EndoC-βH1

To confirm the ACE2 expression in human islets, we also evaluated its transcriptional activity both in collagenase-isolated and in Laser-Capture Microdissected (LCM) human pancreatic islets, by measuring its mRNA expression using TaqMan RT-Real Time PCR. In order to avoid detection of genomic DNA, we used specific primers set generating an amplicon spanning the exons 17-18 junction of ACE2 gene, thus uniquely identifying its mRNA (**Fig. S4A**). Collagenase-isolated human pancreatic islets obtained from 4 different non-diabetic donors pancreata (**Table S1**) showed a medium-level expression of ACE2 mRNA, as demonstrated by RT-Real-Time PCR raw cycle threshold (Ct) values, reporting a Ct range between 28-29 (**Fig. 3A**). Since human pancreatic islets enzymatic isolation procedures may induce some changes in genes expression (Negi et al., 2012), we microdissected human islets from frozen pancreatic tissues obtained from five non-diabetic

multiorgan donors recruited within INNODIA EUnPOD network (Nigi et al., 2020) and evaluated ACE2 mRNA levels. The LCM procedure (**Fig. S4B**) allowed us to extract high quality total RNA (**Fig. S4 C**) from human pancreatic islets directly obtained from their native microenvironment, thus maintaining transcriptional architecture. ACE2 mRNA expression in LCM-human pancreatic islets showed a consistent expression among cases, similar to isolated islets, as shown by ACE2 mRNA raw Ct and normalized values (**Fig. 3B and 3E**).

Finally, we analysed ACE2 mRNA expression in the human β-cell line EndoC-βH1, widely adopted as a model of functional β-cell in diabetes research (Ravassard et al., 2011; Weir and Bonner-Weir, 2011). The analysis of ACE2 mRNA expression in these cells demonstrated a similar expression level in comparison to human pancreatic islets (**Fig. 3 C and 3 F**), with raw Ct values ranging from 27 to 29. In EndoC-βH1, ACE2 immunofluorescence staining showed positive signal in a large majority of the cells (**Fig 3 G, panel -a to panel -h**) and allowed us to track its subcellular localization. Notable, despite ACE2 well-known plasma membrane subcellular localization (Deshotels et al., 2014), we also observed a punctuate and likely granular cytoplasmic signal (**Fig 3 G, panel -c**), in line to what we observed in β-cells of human pancreatic tissues, thus reinforcing the hypothesis of ACE2 protein subcellular localization in β-cell rich insulin secretory granules. Indeed, ACE2-insulin double immunofluorescence staining showed a partial overlap between ACE2 signal and insulin-positive secretory granules (**Fig 3 G, panel h**), implying the existence of ACE2 protein in different compartments of β-cells.

ACE2 expression is increased by pro-inflammatory cytokines in EndoC-βH1 cells and in human pancreatic islets

To determine whether metabolic or inflammatory stress conditions modify pancreatic endocrine β-cells expression of ACE2, we exposed the human β-cell line EndoC-βH1 and human pancreatic islets to metabolic or inflammatory stressors and then evaluated the expression of SARS-CoV-2 main factor ACE2.

Exposure to fatty acid mediated lipotoxicity (2mM palmitate for 24 h) did not significantly modulate ACE2 expression (**Fig. 4A**). In line with these observations, neither primary human islets exposed to palmitate (Cnop et al., 2014) nor human islets isolated from patients affected by type 2 diabetes (Fadista et al., 2014) and evaluated by RNA sequencing showed any increase in ACE2 mRNA expression as compared to the respective controls (respectively 0.9 control vs 0.5 palmitate and 2.4 control vs 3.5 T2D; mean M; not significant). On the other hand, upon 24 h exposure to a typical diabetic pro-inflammatory cytokines mix (IL-1β- IFNγ and TNFα), EndoC-βH1 cells significantly upregulated ACE2 mRNA levels (fold change: 12.3 vs. not treated control, p=0.031) (**Fig. 4A**). The same results were confirmed through immunofluorescence analysis aimed at measuring ACE2 protein levels and subcellular localization in EndoC-βH1 exposed or not to the same proinflammatory condition (**Fig. 4C**). Indeed, we observed a significant increase in ACE2 mean intensity values upon cytokine treatment, confirming the upregulation of ACE2 protein as well (**Fig. 4E**). These results were confirmed using an automated micro-confocal high content images screening system (Boutros et al., 2015) which allowed us to measure ACE2 granular spots intensity in cytokine-treated vs not-treated EndoC-βH1 cells (**Fig 4D** and **Fig 4F**).

In support of the observed increase of ACE2 upon pro-inflammatory stress, RNA sequencing data analysis of EndoC-βH1 cells exposed to IL-1β+IFNγ (48h) or IFNα (18h) further confirmed such increase (**Table S3**). Indeed, we observed a 24.5 and 55.2 fold-increase ($p<0.0001$) in ACE2 mRNA expression in EndoC-βH1 cells treated with IL-1β+IFNγ or with IFNα, respectively. Importantly, the same expression pattern was observed also in human pancreatic islets exposed to the same

cytokines mix, as demonstrated by detecting a 2.4 and 5.1 fold-increase in ACE2 mRNA expression following IL-1β+IFNγ or IFNα treatment respectively ($p<0.0001$) (**Table S3**). Collectively these results demonstrate that ACE2 is upregulated upon exposure to inflammatory, but not metabolic, stressors both in EndoC-βH1 and in human pancreatic islets.

Discussion

In COVID-19 disease clinical complications involving the metabolic/endocrine system are frequently observed. These include critical alterations of glycaemic control in diabetic patients and new-onset hyperglycaemia at admission in individuals without previous clinical history of diabetes. The latter suggests a potential effect of the SARS-CoV-2 on the insulin producing β-cells in the pancreas.

Previous studies suggested that ACE2, the human host cell receptor of SARS-CoV-2 and SARS-CoV, is expressed in the pancreas, which in other tissues has been shown to be a necessary step for infection permissiveness (Hassan et al., 2020; Hou et al., 2020). It has been shown that ACE2 is expressed in pancreatic tissue (Yang et al., 2010). However, an in-depth analysis aimed at evaluating ACE2 expression pattern distribution in human pancreas is still lacking. Here, we adopted multiple technologies to thoroughly analyse presence of ACE2, both at mRNA and protein level, in order to evaluate its expression and localization in human β-cell line EndoC-βH1, in enzymatic- and LCM-isolated primary human pancreatic islets and in pancreatic tissue samples obtained from non-diabetic multiorgan donors from the INNODIA EUnPOD biobank collection.

Previous studies showed that, during mouse pancreas organogenesis, ACE2 has been observed in insulin-producing cells (Wang et al., 2015), while in adult murine endocrine pancreas it is exclusively present in α-cells and in islets microvasculature (Chodavarapu et al., 2016; Xuan et al., 2017). In human adult pancreas, we primarily observed ACE2 in microvasculature component (endothelial cells or pericytes, both in endocrine and exocrine compartments) and in pancreatic islets endocrine cells.

The expression of ACE2 in the pancreatic microvasculature compartment clearly overlaps with CD31 (or PECAM-1) staining pattern, thus demonstrating its microvasculature association. Of interest, although the exocrine pancreas and the pancreatic islets are highly vascularized (El-Gohary et al.,

2012), only a subset of pancreatic endothelial/pericytes cells markedly express ACE2. Additionally, ACE2 expression in exocrine vascular compartment is surprisingly lobular, resembling the heterogeneous staining pattern of several inflammatory markers. The presence of ACE2 in pancreatic endothelial/pericytes cells is highly significative. As a matter of fact, vascular leakage and endothelitis in various organs, were reported as a typical sign of SARS-CoV-2 infection, driving early local inflammation and then to the exacerbation of immune response (Teuwen et al., 2020; Varga et al., 2020). Therefore, a local vascular damage and inflammation due to SARS-CoV-2 direct infection of $ACE2^{+}$ pancreatic endothelial/pericyte cells cannot be excluded and requires additional studies.

The present results indicate that ACE2 in the human pancreas is expressed also in the pancreatic islets and mostly located in β-cells as compared to α-cells. Our data are corroborated by three different RNA-seq datasets analysing human β- and α-cells transcriptome, reporting higher expression of ACE2 mRNA in β-cells in comparison to α-cells (Blodgett et al., 2015; Bramswig et al., 2013; Dorrell et al., 2011) (**Fig. S5**). These datasets fully overlap with our *in-situ* human pancreatic islets results of ACE2 expression pattern.

Human β-cells positivity to ACE2 may highlight their sensitivity to SARS-CoV-2 entry. Such hypothesis is consistent with the known sensitivity of these cells to infection by several enterovirus serotypes. Indeed, multiple evidence from our and other groups (Dotta et al., 2007; Krogvold et al., 2015; Richardson et al., 2009, 2013) showed that enteroviruses are capable to competently infect β-cells but not α-cells (Op de Beeck and Eizirik, 2016; Spagnuolo et al., 2013); these viruses are thus being considered as one of the potential triggering causes of type 1 diabetes (T1D) (Vehik et al., 2019). Of note, it has been previously demonstrated that human β-cells exclusively express virus receptor isoform Coxsackie and adenovirus receptor-SIV (CAR-SIV), making them prone to infection by certain viruses (Ifie et al., 2018). Therefore, it would not be surprising that, under particular

conditions, human β-cells could be directly infected by SARS-CoV-2. In line with this, a very recent report showed that human pancreatic islets can be infected *in vitro* by SARS-CoV-2 (Yang et al., 2020), supporting our observations of a specific tropism of the virus due to ACE2 expression.

Noteworthy, the subcellular localization of ACE2 in β-cells recapitulates what was previously found for the virus receptor CAR-SIV (Ifie et al., 2018). In our dataset, ACE2 protein signal is mostly cytoplasmic/granular and partially overlaps with insulin granules. Such subcellular localization was observed both *in-vitro* in EndoC-βH1 and *ex vivo* in β-cells of primary human pancreatic tissues. Although ACE2 has been primarily observed on cell surfaces in other cell types (Lee et al., 2020; Warner et al., 2005), it should be noted that; (i) upon activation, ACE2 can be internalized through endosome/lysosome pathway (Deshotels et al., 2014); (ii) in β-cells, ACE2 trafficking to cell membrane can be mediated by insulin granules, as previously observed for other integral membrane proteins, such as CAR-SIV (Ifie et al., 2018); (iii) ACE2 can be secreted and found in a soluble form – ACE2 release is enabled by the activity of several proteases that are highly enriched in the insulin granule (Suckale and Solimena, 2010). Therefore, it is possible that ACE2 can be found in different compartments in the same cell type. Of note, it should be mentioned that both SARS-CoV and SARS-CoV-2 can adopt endo-lysosomal organelles pathways to enter host cells (Burkard et al., 2014; Shang et al., 2020), thus rendering of particular interest our findings related to an active trafficking of ACE2 protein in β-cells.

Our data also indicate that in β-cells, ACE2 expression is upregulated upon different pro-inflammatory conditions, but not when exposed to lipotoxic stress. Importantly, these observations were confirmed both in the human beta-cell line EndoC-βH1 and in human primary pancreatic islet cells, as shown by our RNA-seq datasets. As a matter of fact, ACE2 has been previously indicated as an interferon-stimulated gene (ISG) in a variety of cells (Ziegler et al., 2020), including insulin-producing β-cells as shown in the present study. Although additional studies are necessary to clarify

ACE2 expression-related mechanisms, such results may explain at least in part: (*i*) the observed alteration of glycaemic control at admission in SARS-CoV-2 individuals without previous clinical history of diabetes; (*ii*) the increased severity of COVID-19 in those subjects with previous inflammatory-based diseases. The pre-diabetic phase is characterized by high metabolic demand and an elevated inflammatory state (Ferreira et al., 2014; Sims et al., 2020). Such unfavourable inflammatory stresses on pancreatic islets may induce upregulation of ACE2 in β-cells thus rendering them potentially more susceptible to SARS-CoV-2 infection and accelerating β-cell loss.

In conclusion, the presently described preferential expression of ACE2 in human β-cells, alongside with its upregulation under pro-inflammatory conditions, highlights the potential risk for SARS-CoV-2 infection of pancreatic islets. Further mechanistic-based studies and epidemiological evaluation of individuals affected by COVID-19, including long-term clinical follow up and determination of islet autoantibodies, may help to clarify whether human β-cells are among the target cells of SARS-CoV-2 virus and whether β-cell damage, with the potential induction of autoimmunity in genetically susceptible individuals, occurs during and/or after infection.

Acknowledgments

The work is supported by the Innovative Medicines Initiative 2 (IMI2) Joint Undertaking under grant agreement No.115797-INNODIA and No.945268 INNODIA HARVEST. This joint undertaking receives support from the Union's Horizon 2020 research and innovation programme and EFPIA, JDRF and the Leona M. and Harry B. Helmsley Charitable Trust. FD was supported by the Italian Ministry of University and Research (2268-2019-DF-CONRICMIUR-PRIN2017_001). GS was supported by the Italian Ministry of University and Research (2268-2019-SG-CONRICMIUR-PRIN2017_001).

We thank Dr. R. Scharfmann (University of Paris, France) who provided human pancreatic beta cell line EndoC-βH1.

The secretarial help of Maddalena Prencipe and Alessandra Mechini is greatly appreciated.

Author Contributions

GS, FD, DF, GL, NB conceived and designed the experiments. GS, DF, GL and NB performed RT- Real Time PCR, Laser Capture Microdissection and Immunohistochemical/Confocal fluorescence Microscopy analysis experiments. DF and GEG performed EndoC-βH1 cell culture experiments. PM and LM isolated human pancreatic islets and contributed to the collection and processing of human pancreata. LN and NB curated FFPE processing and data analysis of INNODIA EUnPOD pancreata biobank collection. DLE and MC conceived and performed RNA-seq on EndoC-βH1 and human pancreatic islets and contributed to the scientific discussion. CM, CG and LO conceived the experiments and contributed to the scientific discussion. All authors reviewed and provided input to the manuscript.

Declaration of Interests

The authors declare no competing interests

Figure Titles and legends

Figure 1. ACE2 staining pattern in human pancreas. (A) Immunohistochemistry for ACE2 in human pancreatic tissue sections. ACE2 is expressed in endothelial cells or pericytes (panel-a and -b), in some rare ductal cells (panel-c and -d) and in a subset of endocrine cells within pancreatic islets (panel-e and -f). Scale bars in panel-a, -c and -e: 150 µm. Scale bars in panel-b and -f: 70 µm. Scale bars in panel-d: 50 µm. Zoom-in images are reported in panel -b, -d and -f. (**B**) ACE2 expression lobularity in pancreatic endothelial cells/pericytes. Representative image of human pancreatic FFPE section stained for ACE2 in the case 301118. In panel-a, a representative image of a pancreatic section showing two lobules with different staining for ACE2 in endothelial cells/pericytes. In panel-b, a specific segmentation of the two lobules with high (blue) and low or null expression of ACE2 (red) is shown, suggesting lobularity of ACE2 expression in exocrine endothelial cells/pericytes of human pancreas. In panel-c and -d, two zoom insets for high ACE2 expression lobule and low-expressing one is shown, respectively. Scale bar in panel-a: 100 µm. Scale bars in panel-c and -d: 30 µm.

Figure 2. In human pancreatic islets ACE2 is preferentially expressed in insulin-producing β-cells. Triple immunofluorescence staining and image analysis of FFPE human pancreatic section stained for insulin (red), glucagon (blue) and ACE2 (green). (**A**) Representative islets of two different cases. Panel-a to -g: representative pancreatic islet of FFPE pancreas block Body01A of 110118. Panel-h to -m: representative pancreatic islet of FFPE pancreas block Body01B of 141117 case. Panel-e to -g: digital zoom in images of the pancreatic islet reported in panel-d. Panel-l and -m: digital zoom in images of the pancreatic islet reported in panel-k. Scale bar in panel-d and -k: 100 µm. (**B)** Subcellular localization of ACE2 in insulin-positive β-cells of a human pancreatic islets of the case 110118; scale Bar: 10 µm. (**C**) Colocalization rate analysis of overlapping ACE2-insulin and ACE2-glucagon in 128

single pancreatic islets of 7 different cases: p-value was calculated using Wilcoxon matched-pairs signed rank test. On the right: colocalization rate analysis of ACE2-insulin and ACE2-glucagon in each of the 7 cases analysed. For each case, a total of 7-11 islets/section were analysed.

Figure 3. qRT-Real Time PCR analysis of ACE2 mRNA in isolated human pancreatic islets from non-diabetic donors and in the human β-cell line EndoC-βH1. (**A-C**) ACE2 raw Ct values results in enzymatic-isolated human pancreatic islets samples (n=4), in LCM-microdissected islets (n=5) and in EndoC-βH1 (n=4). (**D-F**) ACE2 expression values normalized using GAPDH and β2-microglobulin of the samples analysed in A-C. Values are reported as 2^{-dCt}. Mean ± S.D. values are shown.

(**G**) ACE2 and insulin double immunofluorescence analysis in EndoC-βH1 cultured cells. Negative isotype primary antibody control (relative to ACE2 primary antibody) is shown in panel-a. Insulin (red) and ACE2 (green) are reported in panel-b and -c, while overlay is reported in panel-d. Zoom-in images are reported from panel-e to -h. Scale bar in panel -h = 15 µm.

Figure 4. ACE2 expression is increased by inflammatory stresses. ACE2 mRNA RT-Real-Time PCR analysis in EndoC-βH1 treated or not (CTR) with Palmitate (2,0 mM) (**A**) or with cytokines (IL-1β+IFNγ+TNFα) (Cyt. Mix) (**B**) for 24h. Results are reported as mean ± S.D of 2^{-dCT} normalized values. p-values were calculated using Wilcoxon matched-pairs signed rank test. (**C**) Immunofluorescence analysis of insulin (red, panel-a and -g) and ACE2 (panel-b and -h) in EndoC-βH1 not-treated (panel-a to -f) or treated (panel-g to -l) with cytokines for 24 h. Digital Zoom in images are reported in panel-d to -f and in panel-j to -l. Scale bar in panel-f: 10 µm. Scale bar in panel-l: 15 µm. (**D**) Representative images of ACE2 staining (green) and analysis using micro-confocal High-content screening in EndoC-βH1 treated or not with cytokines (IL-1β+IFNγ+TNFα). Panel-a and -b: ACE2 signal (green) and automated cell cytoplasm segmentation and identification. Panel -c and -d: identification of ACE2 granular spots within segmented cytoplasm in panel-a and -b. Each ACE2 granular spot intensity was

measured and analysed. (**E**) Mean intensity imaging analysis related to experiments in (C) of EndoC-βH1 treated or not with cytokines. Data are reported as individual values alongside with mean ± S.D of RGB grey-intensity measures of 6-11 different experimental points related to two different independent experiments. Individual values alongside with mean ± S.D are reported. P-value was calculated using Mann Whitney U test. (**F**) High content screening analysis of Corrected Median Spot intensity of ACE2 signal in EndoC-βH1 treated or not with cytokines. Median intensity values of 3 different experimental points are reported. P-value was calculated using Mann Whitney U test ($p<0,05$).

STAR Methods

Human donors. Human pancreatic sections analysed in this study were obtained from pancreata collected from brain-dead non-diabetic multiorgan donors within the European Network for Pancreatic Organ Donors with Diabetes (EUnPOD), a project launched in the context of the INNODIA consortium (www.innodia.eu). Following acquisition of informed research consent, pancreata were collected from multiorgan donors. Whole pancreata were processed following standardized procedures at University of Pisa. Formalin fixed paraffin embedded (FFPE) pancreatic tissue sections and frozen OCT pancreatic tissue sections were obtained from n=7 multiorgan donors (**Table S1**). In INNODIA EUnPOD network, pancreata not suitable for organ transplantation were obtained with informed written consent by organ donors' next-of -kin and processed with the approval of the local ethics committee of the Pisa University.

Human pancreatic islets. Human pancreatic islets were obtained from n=4 non-diabetic multi-organ donors (see Supplementary **Table S1**). Briefly, purified islets were prepared by intraductal collagenase solution injection and density gradient purification, as previously described (Gallo et al., 2007). At the end of the isolation procedure, fresh human pancreatic islets preparations were resuspended in CMRL culture medium (cat. 11-530-037, ThermoFisher Scientific, Waltham, MA, USA) supplemented with L-Glutamine 1% (cat. G7513-100ML), Antibiotic/Antimicotic 1% (A5955-100ML, Sigma Aldrich, St. Louis, MO, USA), FBS 10% and cultured at 28°C in a 5% CO_2 incubator.

Cell culture. EndoC-βH1 human β-cell line (Ravassard et al., 2011; Scharfmann et al., 2014) was obtained by UniverCell-Biosolutions (Toulouse-France) and used for all the experiments between passages 78-88. EndoC-βH1 were cultured in coated flasks (coating medium: DMEM high-glucose cat. 51441C, Penicillin/Streptomycin 1% cat. P0781, ECM 1% cat. E1270 and Fibronectin from bovine

plasma 0.2% cat. F1141 - all from Sigma Aldrich, St. Louis, MO, USA) and maintained in culture in low-glucose DMEM (cat. D6046) supplemented with 2% BSA fraction V (cat. 10775835001), β-Mercaptoethanol 50 µM (cat. M7522), L-Glutamine 1% (cat. G7513), Penicillin/Streptomycin 1% (cat. P0781), Nicotinamide 10 mM (cat. N0636), Transferrin 5.5 µg/mL (cat. T8158) and Sodium selenite 6.7 ng/mL (cat. S5261) (all from Sigma Aldrich, St. Louis, MO, USA).

In order to evaluate ACE2 expression in human β cells under diabetogenic stress conditions, EndoC-βH1 cell line was subjected to lipotoxic and inflammatory stresses. Briefly, EndoC-βH1 cells were plated at a density of 1.56×10^5/well in 24 well plates or 40×10^4/well in 96 well plates. After 48 h, lipotoxic and inflammatory stimuli were performed as previously described (Gurgul-Convey et al., 2016; Krizhanovskii et al., 2017). In details, lipotoxic and inflammatory stresses have been induced respectively by 2 mM of Sodium Palmitate (cat. P9767-5G - Sigma Aldrich, St. Louis, MO, USA) or 0,5% EtOH (as control treatment) for 24 h, or cytokines mix IL-1β (50 U/mL) (cat. #201-LB-005 R&D System, Minneapolis, MN, USA), TNFα (1000 U/mL) (cat. T7539 - Sigma Aldrich, St. Louis, MO, USA) and IFNγ (1000 U/mL) (cat. 11040596001- Roche, Basilea, Switzerland) for 24 h.

Laser capture microdissection (LCM). Pancreatic human tissue samples (n=5) from EUnPOD multiorgan donors (**Table S1**) were frozen in Tissue-Tek OCT compound and then 7-µm thick sections were cut from frozen O.C.T. blocks. Sections were fixed in 70% ethanol for 30 s, dehydrated in 100% ethanol for 1 min, in 100% ethanol for 1 min, in xylene for 5 min and finally air-dried for 5 min. Laser capture microdissection (LCM) was performed using an Arcturus XT Laser-Capture Microdissection system (Arcturus Engineering, Mountain View, CA, USA) by melting thermoplastic films mounted on transparent LCM caps (cat. LCM0214 - ThermoFisher Scientific, Waltham, MA, USA) on specific islet areas. Human pancreatic islets were subsequently visualized through islet autofluorescence for LCM procedure. Thermoplastic films containing microdissected cells were incubated with 10 µl of

extraction buffer (cat. kit0204 - ThermoFisher Scientific, Waltham, MA, USA) for 30 min at 42 ◦C and kept at −80°C until RNA extraction. Each microdissection was performed within 30 min from the staining procedure. Overall n=50 microdissected pancreatic islets from each case were analysed.

RNA extraction from LCM isolated human pancreatic islets. Total RNA was extracted from each LCM sample using PicoPure RNA isolation kit Arcturus (cat. kit0204 - ThermoFisher Scientific, Waltham, MA, USA) following manufacturer's procedure. Briefly, the cellular extracts were mixed with 12.5 µl of Ethanol (100%) and transferred to the purification column filter membrane. DNase treatment was performed using RNase-Free DNase Set (cat. 79254 - Qiagen, Hilden, Germany). Total RNA was eluted in 11 µl of DNase/RNase-Free Water and LCM captures deriving from human sample were pooled and subjected to a subsequent concentration through Savant SpeedVac SC100 centrifugal evaporator. Agilent 2100 Bioanalyzer technology with RNA Pico chips (cat. 5067-1513 Agilent Technologies, Santa Clara, CA, USA) was performed for each RNA sample, in order to analyze RNA integrity (RIN) and concentration.

RNA extraction from cells. For genes expression evaluation, total RNA was extracted from approximately $3.0x10^5$ EndoC-βH1 cells using Direct-zol RNA Miniprep Kit (cat. R202-Zymo Research, Irvine, CA, US) following manufacturer's instructions. Briefly, the pelleted cells were resuspended in QIAzol (cat. 79306, Qiagen), mixed with equal volume of Ethanol (100%) and transferred to Zymo-Spin™ IICR Column. DNase digestion was performed using RNase-Free DNase Set (cat. 79254). RNA was eluted in 30 µl of DNase/RNase-Free Water.

RT-Real Time PCR analysis. Total RNA extracted from EndoC-βH1 samples was quantified using Qubit 3000 Fluorometer (ThermoFisher Scientific, Waltham, MA, USA), while those extracted from

LCM-islets were quantified using 2100 Bioanalyzer-RNA 6000 Pico Kit (cat. 50671513, Agilent Technologies, Santa Clara, CA, USA) as well as RNA integrity (RIN). Samples with RIN<5.0 were excluded. Reverse transcriptase reaction was performed using SuperScript™ VILO™ cDNA Synthesis Kit (cat. 11754050- ThermoFisher Scientific, Waltham, MA, USA).

cDNA deriving from LCM human pancreatic islets was then amplified using TaqMan PreAmp Master Mix (cat. 4488593, ThermoFisher Scientific, Waltham, MA, USA) following manufacturer's instructions.

Real-Time PCR analysis was performed using TaqMan gene expression assays using the primers (see Key Resources Table) and SensiFast Probe Lo-ROX Kit (cat.# BIO-84020, Bioline) following manufacturer's recommendation. Data were collected and analysed through Expression Suite software 1.0.1 (ThermoFisher Scientific, Waltham, MA, USA) using $2^{-\Delta Ct}$ or $2^{-\Delta\Delta Ct}$ method. ViiA7 Real-Time PCR thermacycler instrument (ThermoFisher Scientific, Waltham, MA, USA) was used to perform Real-Time PCR reactions.

ACE2 Immunohistochemistry analysis of human pancreatic sections. In order to evaluate the staining pattern of ACE2 in human pancreatic tissues, we analyzed FFPE sections (7 µm thickness) from two different part of FFPE pancreas tissue for each multiorgan donor (listed in **Table S1**), for a total of 14 sections.

After deparaffinization and rehydration through decreasing alcohol series, pancreatic sections were incubated with 1X Phosphate-Buffered Saline with Ca^{2+} and Mg^{2+} (PBS 1X) supplemented with 3% H_2O_2 (cat. H1009 - Sigma Aldrich, St. Louis, MO, USA) to block endogenous peroxidases. Antigen retrieval was performed using 10 mM citrate buffer in microwave (600 W) for 10 minutes, maintaining boiling conditions. Sections were incubated with PBS 1X supplemented with 5% rabbit serum (cat. SCBD33ISV - Sigma Aldrich, St. Louis, MO, USA) to reduce non-specific reactions. Sections

were incubated with primary antibody monoclonal mouse anti-Human ACE2 (cat. MAB933, R&D System, Minneapolis, MN, USA) diluted 1:33 in PBS 1× supplemented with 5% rabbit serum for all night at +4°C. The next day, sections were incubated with secondary antibody polyclonal rabbit anti-mouse HRP-conjugate (cat. P0260, Agilent Technologies, Santa Clara, CA, USA) diluited 1:100 in PBS 1× for 1h at room temperature (RT). Subsequently the sections were incubated with one drop of 3,3' Diaminobenzidine (DAB) chromogen solution (cat. RE7270-K, Novolink MAX DAB, Leica Microsystems, Wetzlar, Germany) for 5 minutes, to trigger the chromatic reaction. Stained sections were then counterstained with hematoxylin (cat. MHS31, Sigma Aldrich, St. Louis, MO, USA) for 4 minutes, for better visualization of the tissue morphology. After the dehydration through increasing alcohol series, the pancreatic sections were mounted with Eukitt mouting medium (cat. S9-25-37, Bio Optica, Milan, Italy) and covered with a coverslip allowing them to dry.

ACE2, insulin and glucagon Immunofluorescence. FFPE pancreatic sections were analysed by triple immunofluorescence in order to evaluate the expression pattern of ACE2, insulin and glucagon. After deparaffinization and rehydration through decreasing alcohol series, pancreatic sections were subjected to antigen retrieval performed using 10 mM citrate buffer in microwave (600W) for 10 minutes. Sections were incubated with PBS 1X supplemented with 3% Bovine Serum Albumin (BSA, cat. A1470-25G, Sigma Aldrich, St. Louis, MO, USA) to reduce non-specific reactions. Then, sections were incubated with primary antibody monoclonal mouse anti-human ACE2 (cat. MAB933, R&D System, Minneapolis, MS, USA) diluted 1:33 in PBS 1X supplemented with 3% BSA, overnight at +4°C. The next day the sections were incubated with polyclonal Rabbit anti-human Glucagon (cat. A0565, Agilent Technologies, Santa Clara, CA, USA) diluted 1:500 in PBS 1X supplemented with 3% BSA, and prediluted polyclonal Guinea Pig anti-human Insulin (cat. IR002 - Agilent Technologies, Santa Clara, CA, USA) as second and third primary antibodies for 1h at room temperature (RT). Subsequently,

the sections were incubated with goat anti-guinea pig Alexa-Fluor 555 conjugate (cat. A21435, Molecular Probe, ThermoFisher Scientific, Waltham, MA, USA) diluted 1:500 in PBS 1X, goat anti-rabbit Alexa-Fluor 647 conjugate (cat. A21245, Molecular Probe, ThermoFisher Scientific, Waltham, MA, USA) diluted 1:500 in PBS 1X and goat anti-mouse 488 conjugate (cat. A11029 - Molecular Probe, ThermoFisher Scientific, Waltham, MA, USA) diluted 1:500 in PBS 1X, as secondary antibodies for 1h. The sections were counterstained with 4',6-Diamidino-2-phenylindole dihydrochloride (DAPI, cat. D8517, Sigma-Aldrich) diluted 1:3000 in PBS 1X; then were mounted with Vectashield antifade medium (cat. H-1000, Vector Laboratories, Burlingame, CA, USA) and analysed immediately or stored at +4°C until ready for confocal image analysis.

Cultured EndoC-βH1 cells were immunostained for ACE2 and insulin as follows. Treated or not-treated cells were fixed in 4% PFA for 10 min, washed for 10 min in 0.1 mol/L glycine, permeabilized in 0,25% Triton-X-100 for 5 min and blocked in 3% BSA+0.05% Triton-X100 in PBS without Ca^{2+} and Mg^{2+} for 30 min. EndoC-βH1 cells were incubated with prediluted antibody polyclonal Guinea Pig anti-Human Insulin (cat. IR002 - Agilent Technologies, Santa Clara, CA, USA) for 1h at RT. Then, washed with PBS without Ca^{2+} and Mg^{2+} and incubated with monoclonal mouse anti-Human ACE2 (cat. MAB933, R&D System, Minneapolis, MS, USA) diluted 1:33 in BSA 1% in PBS without Ca^{2+} and Mg^{2+} with primary or with negative isotype control mouse IgG2a (cat. X0943 - Agilent Technologies, Santa Clara, CA, USA), rinsed with PBS without Ca^{2+} and Mg^{2+}. Then, EndoC-βH1 cells were incubated with goat anti-mouse-488 and goat anti-guinea pig-594 1:500 in 1% BSA in PBS without Ca^{2+} and Mg^{2+}. EndoC-βH1 cells were incubated with 4',6-Diamidino-2-phenylindole dihydrochloride (DAPI, cat. D8517, Sigma Aldrich, St. Louis, MO, USA) diluted 1:3000 in PBS 1X; then were mounted with Vectashield antifade medium (cat. H-1000 - Vector Laboratories, Burlingame, CA, USA) and analysed immediately or stored at +4°C until ready for confocal image analysis.

Image analysis. Images were acquired using Leica TCS SP5 confocal laser scanning microscope system (Leica Microsystems, Wetzlar, Germany). Images were acquired as a single stack focal plane or in z-stack mode capturing multiple focal planes (n=40) for each identified islet or selected representative islets. Sections were scanned and images acquired at 63× magnification. The same confocal microscope setting parameters were applied to all stained sections before image acquisition in order to uniformly collect detected signal related to each channel.

The analysis of colocalization between ACE2-insulin and between ACE2-glucagon were performed using LasAF software (Leica Microsystems, Wetzlar, Germany). The region of interest (ROI) was drawn to calculate the *colocalization rate* (which indicates the extent of colocalization between two different channels and reported as a percentage) as ratio between the colocalization area and the image foreground.

Micro-confocal High-content Screening analysis. Cultured EndoC-βH1 cells were immunostained for ACE2 and insulin as reported above. Cytokines-treated or not-treated cells (see above) were fixed in 4% PFA for 10 min, washed for 10 min in 0.1 mol/L glycine, permeabilized in 0,25% Triton-X-100 for 5 min and blocked in 3% BSA+0.05% Triton-X100 in PBS without Ca^{2+} and Mg^{2+} for 30 min. EndoC-βH1 cells were incubated with antibody polyclonal Guinea Pig anti-Human Insulin (cat. A21435 - Agilent Technologies, Santa Clara, CA, USA) diluted 1:1740 in BSA 1% in PBS without Ca^{2+} and Mg^{2+} and with monoclonal mouse anti-Human ACE2 (cat. MAB933, R&D System, Minneapolis, MS, USA) diluted 1:33 in BSA 1% in PBS without Ca^{2+} and Mg^{2+} for 2h at RT or with negative isotype control mouse IgG2a (cat. X0943 - Agilent Technologies, Santa Clara, CA, USA). Then, EndoC-βH1 cells were washed with PBS without Ca^{2+} and Mg^{2+} and incubated with goat anti-mouse-488 (cat. A11029 - Molecular Probe, ThermoFisher Scientific, Waltham, MA, USA) and goat anti-guinea pig-555 (cat. A21435, Molecular Probe, ThermoFisher Scientific, Waltham, MA, USA) 1:500 in 1% BSA in

PBS without Ca^{2+} and Mg^{2+}. EndoC-βH1 cells were incubated with 4',6-Diamidino-2-phenylindole dihydrochloride (DAPI, cat. D8517, Sigma Aldrich, St. Louis, MO, USA) diluted 1:3000 in PBS 1X; then washed with PBS without Ca^{2+} and Mg^{2+} and analysed immediately. Fluorescence images of EndoC-βH1 cells were analysed using Opera Phenix High Content Screening System (PerkinElmer, Waltham, MA, USA) acquiring multiple images using 63× magnification; nine microscopic areas per well were selected. Automated image analysis was performed using Harmony® High-Content Imaging (PerkinElmer, Waltham, MA, USA), and the intensity of the fluorescence of treated or not-treated cells were measured based on Alexa-555 (insulin) and Alexa-488 (ACE2) fluorochromes. Images were first segmented into nuclei and cytoplasm using the Find Nuclei building block on the DAPI channel and the Find Cytoplasm on the 488 (ACE2) channel. To detect ACE2 signals the Find spots building block was applied to the 488 channel inside the cytoplasm area previously detected. The intensity rate was obtained from the average of the nine areas and values reported as Corrected Spot Intensity (which is the "Mean Spot Intensity" minus "Spot Background Intensity") (Boutros et al., 2015).

RNA sequencing processing and analysis. Total RNA of EndoC-βH1 cells and of pancreatic human islets exposed or not to IFNα or to IL-1β + IFNγ for the indicated time points was obtained and prepared for RNA sequencing as described (Colli et al., 2020; Gonzalez-Duque et al., 2018; Ramos-Rodríguez et al., 2019). The Bioanalyzer System 2100 (Agilent Technologies, Wokingham, UK) was used to evaluate samples quality by determining the RNA integrity number (RIN) values. Only samples presenting RIN values > 9 were analyzed. The obtained libraries were submitted to a second quality control before sequencing on an Illumina HiSeq 2500. The Salmon software version 0.13.2 (Patro et al., 2017) was used to re-analyse our original RNA-seq data (Colli et al., 2020; Gonzalez-Duque et al., 2018; Ramos-Rodríguez et al., 2019) by mapping the sequenced reads to the human

reference transcriptome from GENCODE version 31 (GRCh38) (Frankish et al., 2019) using the quasi-alignment model. Gene expression is represented in Transcripts Per Million (TPM).

The differentially expressed genes were identified with DESeq2 version 1.24.0 (Love et al., 2014). The estimated number of reads obtained from Salmon were used to run the DESeq2 pipeline. In summary, during this approach the DESeq2 normalizes samples based on per-sample sequencing depth and accounting for the presence of intra-sample variability. Next, the data were fit into a negative binomial generalized linear model (GLM) and computes the Wald statistic. Finally, the obtained p-values are adjusted for multiple comparisons using the false discovery rate (FDR) by the Benjamini-Hochberg method (Benjamini and Hochberg, 1995). Genes were considered significantly modified if have an FDR < 0.05.

Statistical analysis. Results were expressed as mean ± SD. Statistical analyses were performed using Graph Pad Prism 8 software. Comparisons between two groups were carried out using Mann-Whitney U test (for non-parametric data) or Wilcoxon matched-pairs signed rank test. Differences were considered significant with p values less than 0.05.

References

Benjamini, Y., and Hochberg, Y. (1995). Controlling the false discovery rate: A practical and powerful approach to multiple testing. Journal of the Royal Statistical Society: Series B (Methodological) *57*, 289–300.

Blodgett, D.M., Nowosielska, A., Afik, S., Pechhold, S., Cura, A.J., Kennedy, N.J., Kim, S., Kucukural, A., Davis, R.J., Kent, S.C., et al. (2015). Novel Observations From Next-Generation RNA Sequencing of Highly Purified Human Adult and Fetal Islet Cell Subsets. Diabetes *64*, 3172–3181.

Boutros, M., Heigwer, F., and Laufer, C. (2015). Microscopy-based high-content screening. Cell *163*, 1314–1325.

Bramswig, N.C., Everett, L.J., Schug, J., Dorrell, C., Liu, C., Luo, Y., Streeter, P.R., Naji, A., Grompe, M., and Kaestner, K.H. (2013). Epigenomic plasticity enables human pancreatic α to β cell reprogramming. J. Clin. Invest. *123*, 1275–1284.

Burkard, C., Verheije, M.H., Wicht, O., van Kasteren, S.I., van Kuppeveld, F.J., Haagmans, B.L., Pelkmans, L., Rottier, P.J.M., Bosch, B.J., and de Haan, C.A.M. (2014). Coronavirus cell entry occurs through the endo-/lysosomal pathway in a proteolysis-dependent manner. PLoS Pathog. *10*, e1004502.

Cao, M., Zhang, D., Wang, Y., Lu, Y., Zhu, X., Li, Y., Xue, H., Lin, Y., Zhang, M., Sun, Y., et al. (2020). Clinical Features of Patients Infected with the 2019 Novel Coronavirus (COVID-19) in Shanghai, China. medRxiv.

Chen, N., Zhou, M., Dong, X., Qu, J., Gong, F., Han, Y., Qiu, Y., Wang, J., Liu, Y., Wei, Y., et al. (2020). Epidemiological and clinical characteristics of 99 cases of 2019 novel coronavirus pneumonia in Wuhan, China: a descriptive study. Lancet *395*, 507–513.

Chodavarapu, H., Chhabra, K.H., Xia, H., Shenoy, V., Yue, X., and Lazartigues, E. (2016). High-fat diet-induced glucose dysregulation is independent of changes in islet ACE2 in mice. Am. J. Physiol. Regul. Integr. Comp. Physiol. *311*, R1223–R1233.

Cnop, M., Abdulkarim, B., Bottu, G., Cunha, D.A., Igoillo-Esteve, M., Masini, M., Turatsinze, J.-V., Griebel, T., Villate, O., Santin, I., et al. (2014). RNA sequencing identifies dysregulation of the human pancreatic islet transcriptome by the saturated fatty acid palmitate. Diabetes *63*, 1978–1993.

Colli, M.L., Ramos-Rodríguez, M., Nakayasu, E.S., Alvelos, M.I., Lopes, M., Hill, J.L.E., Turatsinze, J.-V., Coomans de Brachène, A., Russell, M.A., Raurell-Vila, H., et al. (2020). An integrated multi-omics approach identifies the landscape of interferon-α-mediated responses of human pancreatic beta cells. Nat. Commun. *11*, 2584.

Deshotels, M.R., Xia, H., Sriramula, S., Lazartigues, E., and Filipeanu, C.M. (2014). Angiotensin II mediates angiotensin converting enzyme type 2 internalization and degradation through an angiotensin II type I receptor-dependent mechanism. Hypertension *64*, 1368–1375.

Dorrell, C., Schug, J., Lin, C.F., Canaday, P.S., Fox, A.J., Smirnova, O., Bonnah, R., Streeter, P.R., Stoeckert, C.J., Kaestner, K.H., et al. (2011). Transcriptomes of the major human pancreatic cell types. Diabetologia *54*, 2832–2844.

Dotta, F., Censini, S., van Halteren, A.G.S., Marselli, L., Masini, M., Dionisi, S., Mosca, F., Boggi, U., Muda, A.O., Del Prato, S., et al. (2007). Coxsackie B4 virus infection of beta cells and natural killer cell insulitis in recent-onset type 1 diabetic patients. Proc. Natl. Acad. Sci. USA *104*, 5115–5120.

El-Gohary, Y., Tulachan, S., Branca, M., Sims-Lucas, S., Guo, P., Prasadan, K., Shiota, C., and Gittes, G.K. (2012). Whole-mount imaging demonstrates hypervascularity of the pancreatic ducts and other pancreatic structures. Anat Rec (Hoboken) *295*, 465–473.

Fadista, J., Vikman, P., Laakso, E.O., Mollet, I.G., Esguerra, J.L., Taneera, J., Storm, P., Osmark, P., Ladenvall, C., Prasad, R.B., et al. (2014). Global genomic and transcriptomic analysis of human pancreatic islets reveals novel genes influencing glucose metabolism. Proc. Natl. Acad. Sci. USA *111*, 13924–13929.

Ferreira, R.C., Guo, H., Coulson, R.M.R., Smyth, D.J., Pekalski, M.L., Burren, O.S., Cutler, A.J., Doecke, J.D., Flint, S., McKinney, E.F., et al. (2014). A type I interferon transcriptional signature precedes autoimmunity in children genetically at risk for type 1 diabetes. Diabetes *63*, 2538–2550.

Frankish, A., Diekhans, M., Ferreira, A.-M., Johnson, R., Jungreis, I., Loveland, J., Mudge, J.M., Sisu, C., Wright, J., Armstrong, J., et al. (2019). GENCODE reference annotation for the human and mouse genomes. Nucleic Acids Res. *47*, D766–D773.

Gallo, R., Gambelli, F., Gava, B., Sasdelli, F., Tellone, V., Masini, M., Marchetti, P., Dotta, F., and Sorrentino, V. (2007). Generation and expansion of multipotent mesenchymal progenitor cells from cultured human pancreatic islets. Cell Death Differ. *14*, 1860–1871.

Gonzalez-Duque, S., Azoury, M.E., Colli, M.L., Afonso, G., Turatsinze, J.-V., Nigi, L., Lalanne, A.I., Sebastiani, G., Carré, A., Pinto, S., et al. (2018). Conventional and Neo-antigenic Peptides Presented by β Cells Are Targeted by Circulating Naïve CD8+ T Cells in Type 1 Diabetic and Healthy Donors. Cell Metab. *28*, 946–960.e6.

Guan, W.-J., Liang, W.-H., Zhao, Y., Liang, H.-R., Chen, Z.-S., Li, Y.-M., Liu, X.-Q., Chen, R.-C., Tang, C.-L., Wang, T., et al. (2020). Comorbidity and its impact on 1590 patients with COVID-19 in China: a nationwide analysis. Eur. Respir. J. *55*.

Gupta, R., Hussain, A., and Misra, A. (2020). Diabetes and COVID-19: evidence, current status and unanswered research questions. Eur. J. Clin. Nutr.

Gurgul-Convey, E., Mehmeti, I., Plötz, T., Jörns, A., and Lenzen, S. (2016). Sensitivity profile of the human EndoC-βH1 beta cell line to proinflammatory cytokines. Diabetologia *59*, 2125–2133.

Hamming, I., Timens, W., Bulthuis, M.L.C., Lely, A.T., Navis, G.J., and van Goor, H. (2004). Tissue distribution of ACE2 protein, the functional receptor for SARS coronavirus. A first step in understanding SARS pathogenesis. J. Pathol. *203*, 631–637.

Hassan, A.O., Case, J.B., Winkler, E.S., Thackray, L.B., Kafai, N.M., Bailey, A.L., McCune, B.T., Fox, J.M., Chen, R.E., Alsoussi, W.B., et al. (2020). A SARS-CoV-2 Infection Model in Mice Demonstrates Protection by Neutralizing Antibodies. Cell.

Hikmet, F., Mear, L., Uhlen, M., and Lindskog, C. (2020). The protein expression profile of ACE2 in human tissues. BioRxiv.

Hou, Y.J., Okuda, K., Edwards, C.E., Martinez, D.R., Asakura, T., Dinnon, K.H., Kato, T., Lee, R.E., Yount, B.L., Mascenik, T.M., et al. (2020). SARS-CoV-2 Reverse Genetics Reveals a Variable Infection Gradient in the Respiratory Tract. Cell.

Iacobellis, G., Penaherrera, C.A., Bermudez, L.E., and Bernal Mizrachi, E. (2020). Admission hyperglycemia and radiological findings of SARS-CoV2 in patients with and without diabetes. Diabetes Res. Clin. Pract. *164*, 108185.

Ifie, E., Russell, M.A., Dhayal, S., Leete, P., Sebastiani, G., Nigi, L., Dotta, F., Marjomäki, V., Eizirik, D.L., Morgan, N.G., et al. (2018). Unexpected subcellular distribution of a specific isoform of the Coxsackie and adenovirus receptor, CAR-SIV, in human pancreatic beta cells. Diabetologia *61*, 2344–2355.

Krizhanovskii, C., Kristinsson, H., Elksnis, A., Wang, X., Gavali, H., Bergsten, P., Scharfmann, R., and Welsh, N. (2017). EndoC-βH1 cells display increased sensitivity to sodium palmitate when cultured in DMEM/F12 medium. Islets *9*, e1296995.

Krogvold, L., Edwin, B., Buanes, T., Frisk, G., Skog, O., Anagandula, M., Korsgren, O., Undlien, D., Eike, M.C., Richardson, S.J., et al. (2015). Detection of a low-grade enteroviral infection in the islets of langerhans of living patients newly diagnosed with type 1 diabetes. Diabetes *64*, 1682–1687.

Lan, J., Ge, J., Yu, J., Shan, S., Zhou, H., Fan, S., Zhang, Q., Shi, X., Wang, Q., Zhang, L., et al. (2020). Structure of the SARS-CoV-2 spike receptor-binding domain bound to the ACE2 receptor. Nature *581*, 215–220.

Lee, I.T., Nakayama, T., Wu, C.-T., Goltsev, Y., Jiang, S., Gall, P.A., Liao, C.-K., Shih, L.-C., Schurch, C.M., McIlwain, D.R., et al. (2020). Robust ACE2 protein expression localizes to the motile cilia of the respiratory tract epithelia and is not increased by ACE inhibitors or angiotensin receptor blockers. medRxiv.

Letko, M., Marzi, A., and Munster, V. (2020). Functional assessment of cell entry and receptor usage for SARS-CoV-2 and other lineage B betacoronaviruses. Nat. Microbiol. *5*, 562–569.

Li, M.-Y., Li, L., Zhang, Y., and Wang, X.-S. (2020). Expression of the SARS-CoV-2 cell receptor gene ACE2 in a wide variety of human tissues. Infect Dis Poverty *9*, 45.

Love, M.I., Huber, W., and Anders, S. (2014). Moderated estimation of fold change and' ' dispersion for RNA-seq data with DESeq2. Genome Biol. *15*, 550.

Mossel, E.C., Huang, C., Narayanan, K., Makino, S., Tesh, R.B., and Peters, C.J. (2005). Exogenous ACE2 expression allows refractory cell lines to support severe acute respiratory syndrome coronavirus replication. J. Virol. *79*, 3846–3850.

Negi, S., Jetha, A., Aikin, R., Hasilo, C., Sladek, R., and Paraskevas, S. (2012). Analysis of beta-cell gene expression reveals inflammatory signaling and evidence of dedifferentiation following human islet isolation and culture. PLoS One *7*, e30415.

Nigi, L., Maccora, C., Dotta, F., and Sebastiani, G. (2020). From immunohistological to anatomical alterations of human pancreas in type 1 diabetes: New concepts on the stage. Diabetes Metab Res Rev *36*, e3264.

Op de Beeck, A., and Eizirik, D.L. (2016). Viral infections in type 1 diabetes mellitus--why the β cells? Nat. Rev. Endocrinol. *12*, 263–273.

Patro, R., Duggal, G., Love, M.I., Irizarry, R.A., and Kingsford, C. (2017). Salmon provides fast and bias-aware quantification of transcript expression. Nat. Methods *14*, 417–419.

Ramos-Rodríguez, M., Raurell-Vila, H., Colli, M.L., Alvelos, M.I., Subirana-Granés, M., Juan-Mateu, J., Norris, R., Turatsinze, J.-V., Nakayasu, E.S., Webb-Robertson, B.-J.M., et al. (2019). The impact of proinflammatory cytokines on the β-cell regulatory landscape provides insights into the genetics of type 1 diabetes. Nat. Genet. *51*, 1588–1595.

Ravassard, P., Hazhouz, Y., Pechberty, S., Bricout-Neveu, E., Armanet, M., Czernichow, P., and Scharfmann, R. (2011). A genetically engineered human pancreatic β cell line exhibiting glucose-inducible insulin secretion. J. Clin. Invest. *121*, 3589–3597.

Richardson, S.J., Willcox, A., Bone, A.J., Foulis, A.K., and Morgan, N.G. (2009). The prevalence of enteroviral capsid protein vp1 immunostaining in pancreatic islets in human type 1 diabetes. Diabetologia *52*, 1143–1151.

Richardson, S.J., Leete, P., Bone, A.J., Foulis, A.K., and Morgan, N.G. (2013). Expression of the enteroviral capsid protein VP1 in the islet cells of patients with type 1 diabetes is associated with induction of protein kinase R and downregulation of Mcl-1. Diabetologia *56*, 185–193.

Rubino, F., Amiel, S.A., Zimmet, P., Alberti, G., Bornstein, S., Eckel, R.H., Mingrone, G., Boehm, B., Cooper, M.E., Chai, Z., et al. (2020). New-Onset Diabetes in Covid-19. N. Engl. J. Med.

Sardu, C., D'Onofrio, N., Balestrieri, M.L., Barbieri, M., Rizzo, M.R., Messina, V., Maggi, P., Coppola, N., Paolisso, G., and Marfella, R. (2020). Outcomes in Patients With Hyperglycemia Affected by Covid-19: Can We Do More on Glycemic Control? Diabetes Care.

Scharfmann, R., Pechberty, S., Hazhouz, Y., von Bülow, M., Bricout-Neveu, E., Grenier-Godard, M., Guez, F., Rachdi, L., Lohmann, M., Czernichow, P., et al. (2014). Development of a conditionally immortalized human pancreatic β cell line. J. Clin. Invest. *124*, 2087–2098.

Shang, J., Wan, Y., Luo, C., Ye, G., Geng, Q., Auerbach, A., and Li, F. (2020). Cell entry mechanisms of SARS-CoV-2. Proc. Natl. Acad. Sci. USA *117*, 11727–11734.

Sims, E.K., Mirmira, R.G., and Evans-Molina, C. (2020). The role of beta-cell dysfunction in early type 1 diabetes. Curr Opin Endocrinol Diabetes Obes *27*, 215–224.

Spagnuolo, I., Patti, A., Sebastiani, G., Nigi, L., and Dotta, F. (2013). The case for virus-induced type 1 diabetes. Curr Opin Endocrinol Diabetes Obes *20*, 292–298.

Suckale, J., and Solimena, M. (2010). The insulin secretory granule as a signaling hub. Trends Endocrinol. Metab. *21*, 599–609.

Teuwen, L.-A., Geldhof, V., Pasut, A., and Carmeliet, P. (2020). COVID-19: the vasculature unleashed. Nat. Rev. Immunol. *20*, 389–391.

Varga, Z., Flammer, A.J., Steiger, P., Haberecker, M., Andermatt, R., Zinkernagel, A.S., Mehra, M.R., Schuepbach, R.A., Ruschitzka, F., and Moch, H. (2020). Endothelial cell infection and endotheliitis in COVID-19. Lancet *395*, 1417–1418.

Vehik, K., Lynch, K.F., Wong, M.C., Tian, X., Ross, M.C., Gibbs, R.A., Ajami, N.J., Petrosino, J.F., Rewers, M., Toppari, J., et al. (2019). Prospective virome analyses in young children at increased genetic risk for type 1 diabetes. Nat. Med. *25*, 1865–1872.

Wang, L., Liang, J., and Leung, P.S. (2015). The ACE2/Ang-(1-7)/Mas Axis Regulates the Development of Pancreatic Endocrine Cells in Mouse Embryos. PLoS One *10*, e0128216.

Wang, S., Guo, F., Liu, K., Wang, H., Rao, S., Yang, P., and Jiang, C. (2008). Endocytosis of the receptor-binding domain of SARS-CoV spike protein together with virus receptor ACE2. Virus Res. *136*, 8–15.

Warner, F.J., Lew, R.A., Smith, A.I., Lambert, D.W., Hooper, N.M., and Turner, A.J. (2005). Angiotensin-converting enzyme 2 (ACE2), but not ACE, is preferentially localized to the apical surface of polarized kidney cells. J. Biol. Chem. *280*, 39353–39362.

Weir, G.C., and Bonner-Weir, S. (2011). Finally! A human pancreatic β cell line. J. Clin. Invest. *121*, 3395–3397.

Wu, J., Huang, J., Zhu, G., Wang, Q., Lv, Q., Huang, Y., Yu, Y., Si, X., Yi, H., Wang, C., et al. (2020). Elevation of blood glucose level predicts worse outcomes in hospitalized patients with COVID-19: a retrospective cohort study. BMJ Open Diabetes Res. Care *8*.

Xuan, X., Gao, F., Ma, X., Huang, C., Deng, H., Wang, S., Li, W., and Yuan, L. (2017). Activation of ACE2/angiotensin (1-7) attenuates pancreatic β cell dedifferentiation in a high-fat-diet mouse model. Metab. Clin. Exp. *81*, 83–96.

Yang, J.-K., Lin, S.-S., Ji, X.-J., and Guo, L.-M. (2010). Binding of SARS coronavirus to its receptor damages islets and causes acute diabetes. Acta Diabetol. *47*, 193–199.

Yang, L., Han, Y., Nilsson-Payant, B.E., Gupta, V., Wang, P., Duan, X., Tang, X., Zhu, J., Zhao, Z., Jaffré, F., et al. (2020). A Human Pluripotent Stem Cell-based Platform to Study SARS-CoV-2 Tropism and Model Virus Infection in Human Cells and Organoids. Cell Stem Cell.

Zhou, P., Yang, X.-L., Wang, X.-G., Hu, B., Zhang, L., Zhang, W., Si, H.-R., Zhu, Y., Li, B., Huang, C.-L., et al. (2020). A pneumonia outbreak associated with a new coronavirus of probable bat origin. Nature *579*, 270–273.

Zhu, L., She, Z.-G., Cheng, X., Qin, J.-J., Zhang, X.-J., Cai, J., Lei, F., Wang, H., Xie, J., Wang, W., et al. (2020). Association of Blood Glucose Control and Outcomes in Patients with COVID-19 and Pre-existing Type 2 Diabetes. Cell Metab. *31*, 1068–1077.e3.

Ziegler, C.G.K., Allon, S.J., Nyquist, S.K., Mbano, I.M., Miao, V.N., Tzouanas, C.N., Cao, Y., Yousif, A.S., Bals, J., Hauser, B.M., et al. (2020). SARS-CoV-2 Receptor ACE2 Is an Interferon-Stimulated Gene in Human Airway Epithelial Cells and Is Detected in Specific Cell Subsets across Tissues. Cell *181*, 1016–1035.e19.

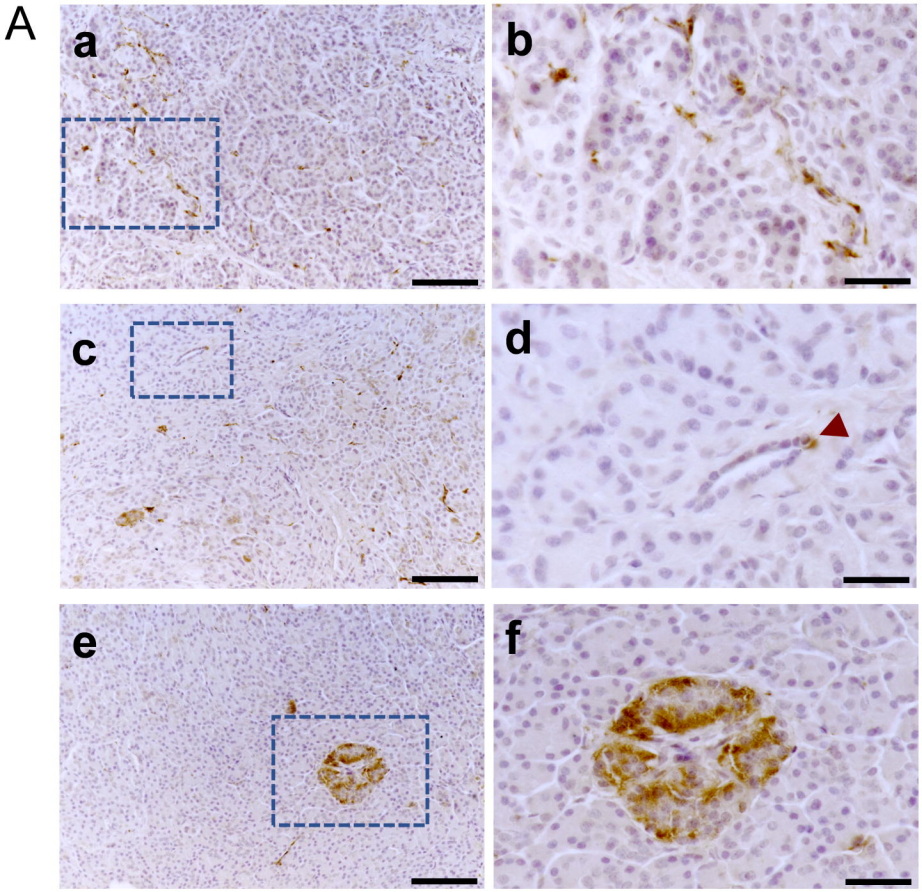
A
a
b
c
d
e
f

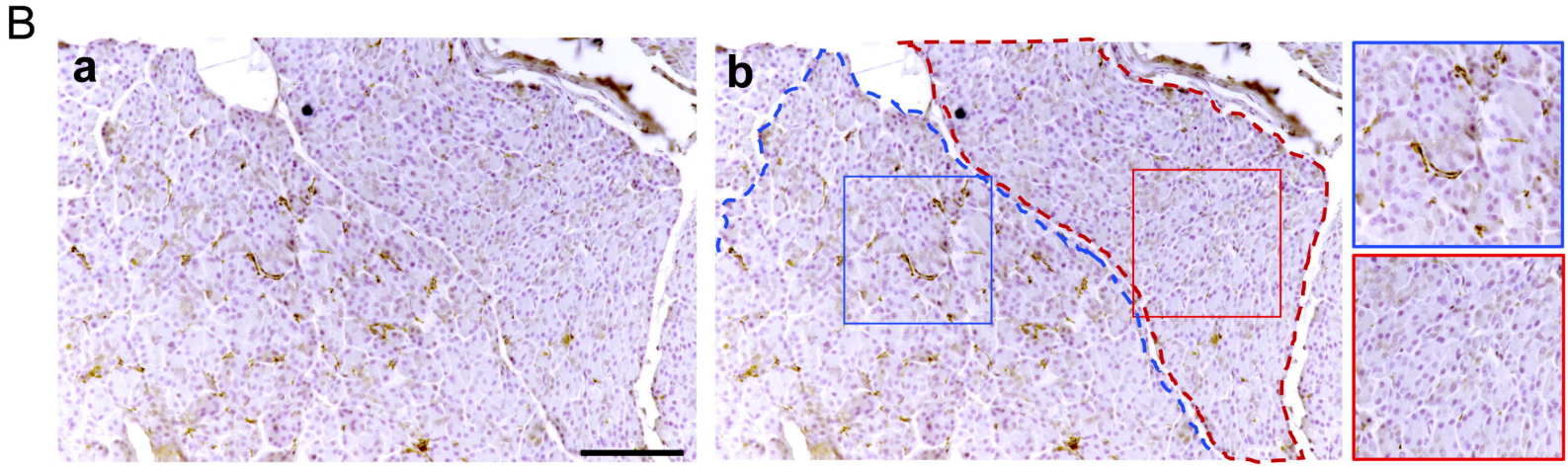
B
a
b

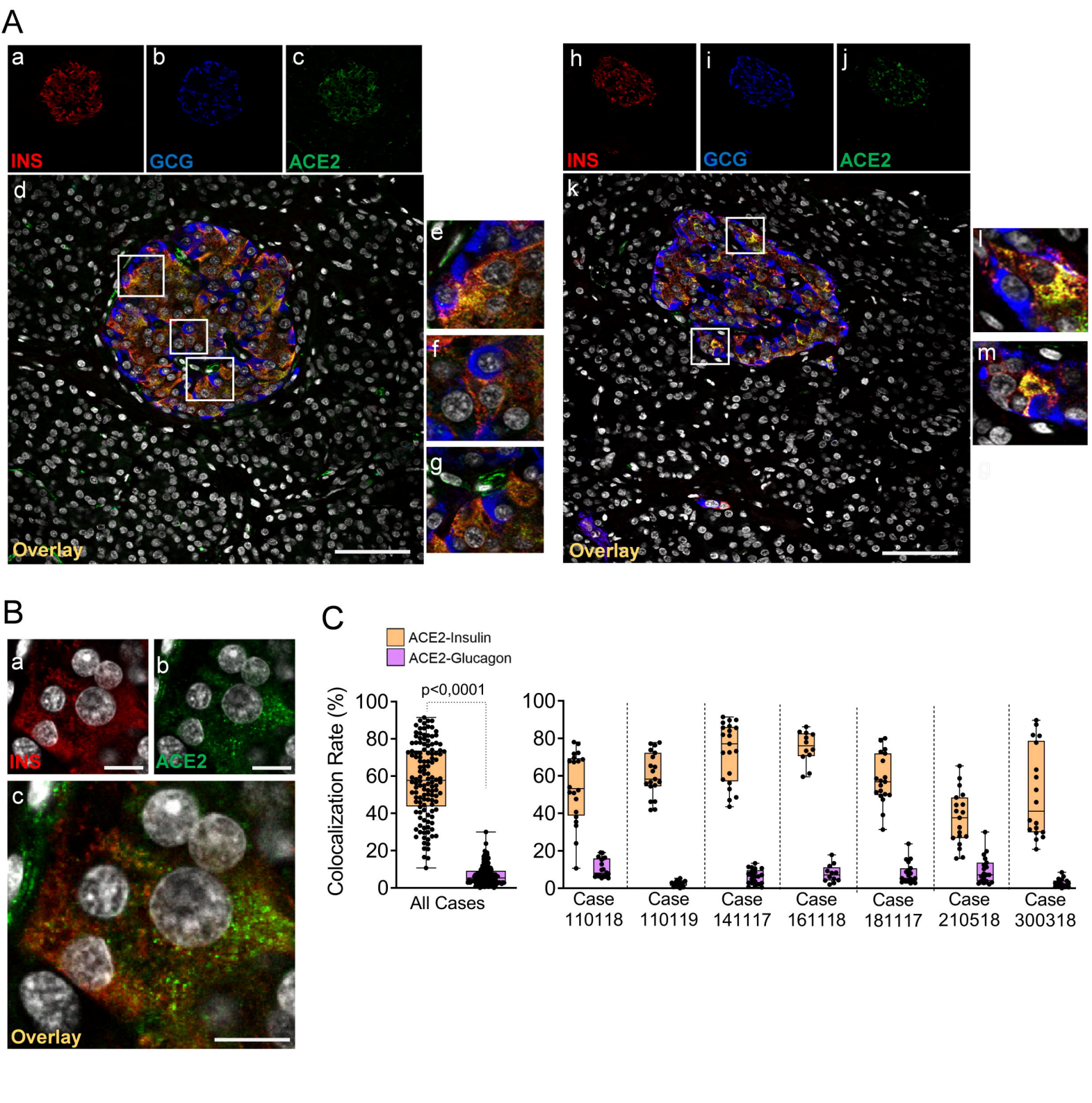
A
a
b
c
INS
GCG
ACE2
d
e
f
g
Overlay
h
i
j
INS
GCG
ACE2
k
l
m
Overlay
B
a
b
INS
ACE2
c
Overlay
C
ACE2-Insulin
ACE2-Glucagon
p<0,0001
Colocalization Rate (%)
100
80
60
40
20
0
All Cases
Case 110118
Case 110119
Case 141117
Case 161118
Case 181117
Case 210518
Case 300318

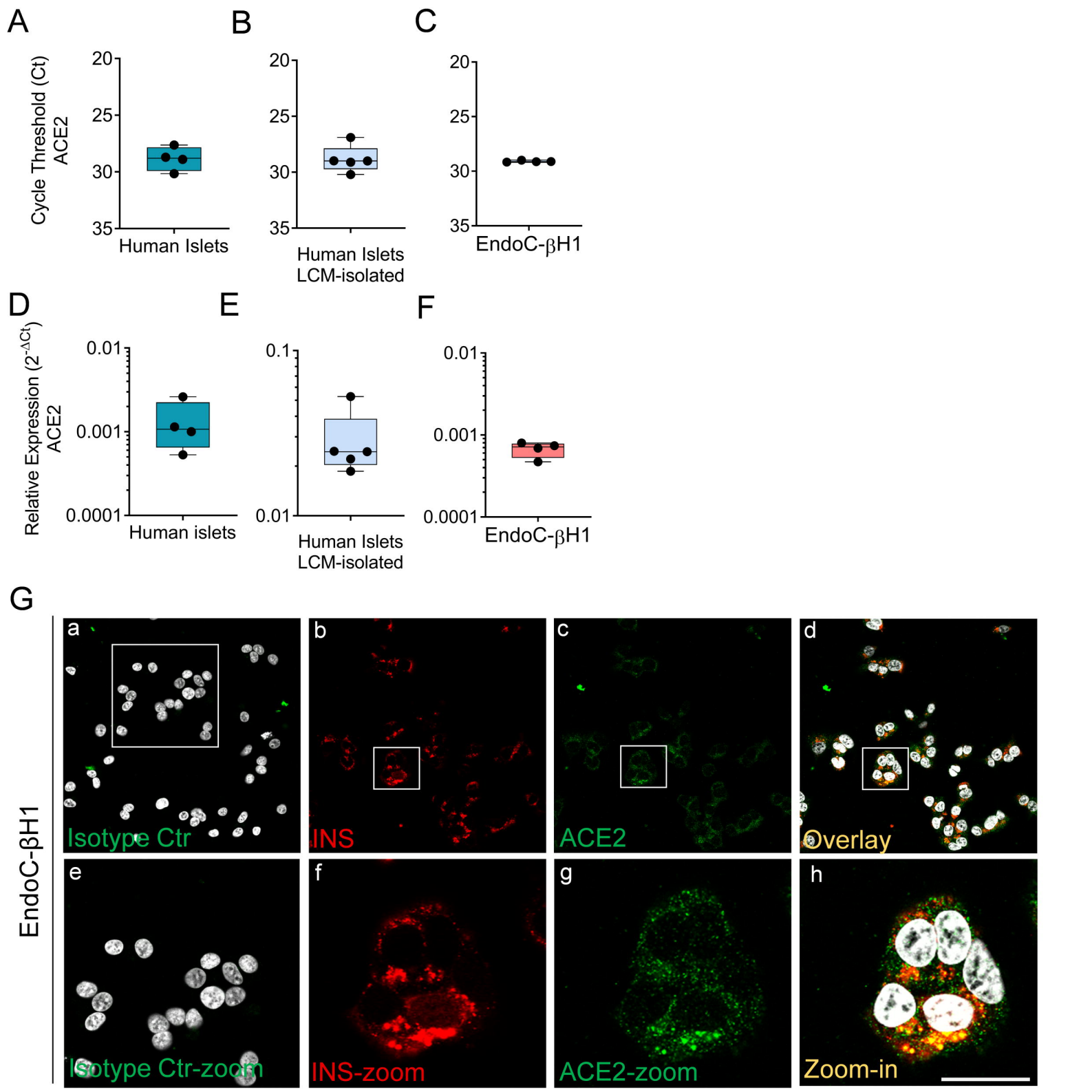
A
B
C
Cycle Threshold (Ct)
ACE2
20
25
30
35
Human Islets
Human Islets
LCM-isolated
EndoC-βH1
D
E
F
Relative Expression ($2^{-\Delta Ct}$)
ACE2
0.01
0.001
0.0001
0.1
Human islets
Human Islets
LCM-isolated
EndoC-βH1
G
EndoC-βH1
a
b
c
d
Isotype Ctr
INS
ACE2
Overlay
e
f
g
h
Isotype Ctr-zoom
INS-zoom
ACE2-zoom
Zoom-in

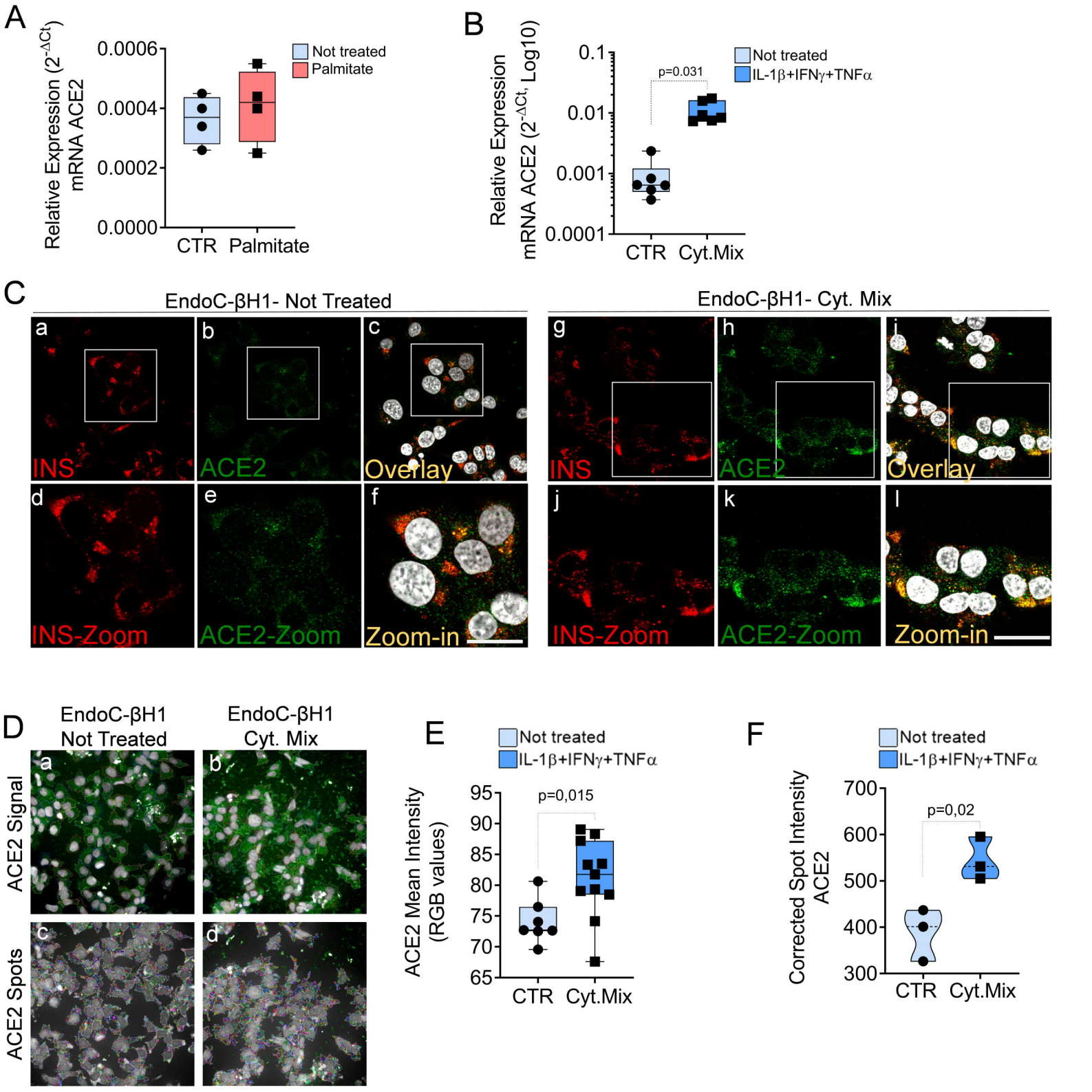
A
Relative Expression ($2^{-\Delta Ct}$) mRNA ACE2
0.0006
0.0004
0.0002
0.0000
Not treated
Palmitate
CTR
Palmitate
B
Relative Expression mRNA ACE2 ($2^{-\Delta Ct}$, Log10)
0.1
0.01
0.001
0.0001
p=0.031
Not treated
IL-1β+IFNγ+TNFα
CTR
Cyt.Mix
C
EndoC-βH1- Not Treated
EndoC-βH1- Cyt. Mix
a
b
c
g
h
i
INS
ACE2
Overlay
INS
ACE2
Overlay
d
e
f
j
k
l
INS-Zoom
ACE2-Zoom
Zoom-in
INS-Zoom
ACE2-Zoom
Zoom-in
D
EndoC-βH1 Not Treated
EndoC-βH1 Cyt. Mix
ACE2 Signal
ACE2 Spots
a
b
c
d
E
Not treated
IL-1β+IFNγ+TNFα
ACE2 Mean Intensity (RGB values)
95
90
85
80
75
70
65
p=0,015
CTR
Cyt.Mix
F
Not treated
IL-1β+IFNγ+TNFα
Corrected Spot Intensity ACE2
700
600
500
400
300
p=0,02
CTR
Cyt.Mix